Comput. Methods Appl. Mech. Engrg. 273 (2014) 100–118

Contents lists available at ScienceDirect

Comput. Methods Appl. Mech. Engrg.

journal homepage: www.elsevier.com/locate/cma

# A higher-order phase-field model for brittle fracture: Formulation and analysis within the isogeometric analysis framework

Michael J. Borden [a,*], Thomas J.R. Hughes [a], Chad M. Landis [b], Clemens V. Verhoosel [c]

[a] Institute for Computational Engineering and Sciences, The University of Texas at Austin, 201 East 24th St. Stop C0200, Austin, TX 78712, USA
[b] Aerospace Engineering and Engineering Mechanics, The University of Texas at Austin, 210 East 24th St. Stop C0600, Austin, TX 78712, USA
[c] Eindhoven University of Technology, Mechanical Engineering, Multiscale Engineering Fluid Dynamics, PO Box 513, 5600 MB Eindhoven, The Netherlands

ARTICLE INFO

*Article history:*
Received 2 August 2013
Received in revised form 21 November 2013
Accepted 21 January 2014
Available online 5 February 2014

*Keywords:*
Phase-field
Fracture
Isogeometric analysis
Higher-order models

ABSTRACT

Phase-field models based on the variational formulation for brittle fracture have recently been gaining popularity. These models have proven capable of accurately and robustly predicting complex crack behavior in both two and three dimensions. In this work we propose a fourth-order model for the phase-field approximation of the variational formulation for brittle fracture. We derive the thermodynamically consistent governing equations for the fourth-order phase-field model by way of a variational principle based on energy balance assumptions. The resulting model leads to higher regularity in the exact phase-field solution, which can be exploited by the smooth spline function spaces utilized in isogeometric analysis. This increased regularity improves the convergence rate of the numerical solution and opens the door to higher-order convergence rates for fracture problems. We present an analysis of our proposed theory and numerical examples that support this claim. We also demonstrate the robustness of the model in capturing complex three-dimensional crack behavior.



## 1. Introduction

Computation often plays a key role in understanding and predicting fracture and failure in materials. Computational models allow fracture processes to be studied in situations where experiments are impractical or impossible. In order for fracture models to be reliable, however, they must be accurate and robust. Much work has been done to develop such models. Many of these models take an approach similar to Griffith's model of brittle fracture where the energy required to create a unit area of fracture surface is equal to some critical value.

The numerical solutions of fracture models typically rely on some type of finite element implementation. The most popular approaches introduce discontinuities into the displacement field by means of remeshing or by enriching the basis by inserting discontinuities using the partition of unity method proposed by Babuška and Melenk [3]. Examples include the extended finite element method introduced by Moës et al. [32], the cohesive zone (or inter element crack) method introduced by Xu and Needleman [40] and Camacho and Ortiz [14], and the cohesive segments methods introduced by Remmers et al.

* Corresponding author. Tel.: +1 5125379335.
*E-mail address:* mborden@ices.utexas.edu (M.J. Borden).

http://dx.doi.org/10.1016/j.cma.2014.01.016
0045-7825/

[34]. These approaches have been studied in depth and have shown much success in modeling many crack propagation problems. Robust extensions of these models to complex three-dimensional problems, however, has proven to be difficult.

An alternative to these models that has been gaining popularity over the last decade is the variational approach to brittle fracture proposed by Francfort and Marigo [19]. In this approach the solution to the fracture problem is found as the minimizer of a global energy functional. The numerical solution of this model relies on the phase-field implementation introduced by Bourdin et al. [10] and is based on an approximate potential developed by Mumford and Shah [33]. A major advantage of this approach is that the fracture problem is reformulated as a system of partial differential equations that completely determine the evolution of the cracks. There are no ad hoc rules or conditions needed to determine crack nucleation, propagation, or bifurcation. This approach has proven to accurately and robustly capture crack behavior in both two and three dimensions as reported by Miehe et al. [30] and Miehe et al. [31], among others. It has also been extended successfully to dynamic problems by Borden et al. [6], Bourdin et al. [11], Hofacker and Miehe [22], Larsen [26] and Larsen and Ortner [27].

In this work we seek to extend the variational approach to brittle fracture by proposing a fourth-order model for the phase-field approximation. Our model includes higher-derivative terms for the phase-field that lead to greater regularity of the exact solution. This solution regularity improves the convergence rate and accuracy of the numerical solution. To solve the higher-order problem we use the isogeometric analysis framework proposed by Hughes et al. [24]. Isogeometric analysis provides an efficient, smooth basis for computation. Once the problem is recast in terms of the isogeometric analysis framework, the additional smoothness requirements are met with minimal computational cost.

To justify our model, we provide numerical analyses and results that show improved convergence rates for key quantities when comparing our fourth-order model to the existing model. We also provide numerical examples that demonstrates the capability of the model to robustly capture complex three-dimensional crack behavior.

The paper will proceed as follows. In Section 2 we will establish notation, review the existing phase-field formulation for the variational description of brittle fracture, and introduce a new fourth-order phase-field formulation. The formulation will be derived from an energy balance principle. Section 3 will present an analysis of the formulations established in Section 2. We will begin with a simple one-dimensional analysis that will show improved convergence properties for the fourth-order formulation. This will be followed by a numerical study of a two-dimensional problem that will help to verify the results of the one-dimensional analysis. This section will conclude with a three-dimensional example that demonstrates the ability of phase-field models to capture complex three-dimensional crack behavior. In Section 4 we will summarize our results and conclusions.

## 2. Formulation

In this section we first introduce definitions and notations and then derive the fourth-order phase-field model. We let $\Omega \subset \mathbb{R}^d$ (with $d \in \{1,2,3\}$) be an arbitrary body with external boundary $\partial\Omega$ and internal discontinuity boundary $\Gamma$. The displacement of a point $\mathbf{x}$ at time $t$ is denoted by $\mathbf{u}(\mathbf{x},t)$. The displacement field satisfies time-dependent Dirichlet boundary conditions, $\mathbf{u}(\mathbf{x},t) = \mathbf{g}(\mathbf{x},t)$, on $\partial\Omega_{\mathbf{g}} \subseteq \partial\Omega$, and time-dependent Neumann (i.e., traction) boundary conditions on $\partial\Omega_{\mathbf{h}} \subseteq \partial\Omega$, where $\overline{\partial\Omega_{\mathbf{g}} \cup \partial\Omega_{\mathbf{h}}} = \partial\Omega$. We assume small strains throughout the paper. The usual small strain tensor, $\boldsymbol{\varepsilon}(\mathbf{x},t) \in \mathbb{R}^{d\times d}$, is defined by

$$\boldsymbol{\varepsilon} = \operatorname{symm}[\nabla \mathbf{u}]. \tag{1}$$

We assume isotropic linear elasticity, such that the undamaged elastic energy density is given by

$$\psi_e(\boldsymbol{\varepsilon}) = \frac{1}{2}\lambda \operatorname{tr}(\boldsymbol{\varepsilon})^2 + \mu \boldsymbol{\varepsilon} : \boldsymbol{\varepsilon}, \tag{2}$$

where $\lambda$ and $\mu$ are the Lamé constants.

### 2.1. Phase-field approximations of the variational description of fracture

The evolving internal discontinuity boundary, $\Gamma(t)$, represents a set of discrete cracks. In accordance with energetic approaches to fracture, the energy required to create a unit area of fracture surface is equal to the critical fracture energy density $\mathcal{G}_c$. The total potential energy of the body, $\Psi$, is then given by

$$\Psi(\boldsymbol{\varepsilon},\Gamma) = \int_\Omega \psi_e(\boldsymbol{\varepsilon})\, d\Omega + \int_\Gamma \mathcal{G}_c\, d\Gamma, \tag{3}$$

where $\psi_e$ is the elastic strain energy density function and the fracture energy contribution is merely the critical fracture energy density, $\mathcal{G}_c$, integrated over the fracture surface. Irreversibility of the fracture process dictates that $\Gamma(t) \subseteq \Gamma(t+\Delta t)$ for all $\Delta t > 0$. Hence, translation of cracks through the domain is prohibited, but cracks can extend, branch, and merge.

The variational approach to fracture proposed by Francfort and Marigo [19] predicts the nucleation, propagation and interaction of cracks by finding a global minimizer of (3). Solving this variational problem numerically for discrete cracks can be difficult because the crack path, $\Gamma$, is evolving with time. In order to circumvent this difficulty, Bourdin et al. [10] introduced a volumetric approximation to the surface integral. This approximation uses a continuous scalar-valued

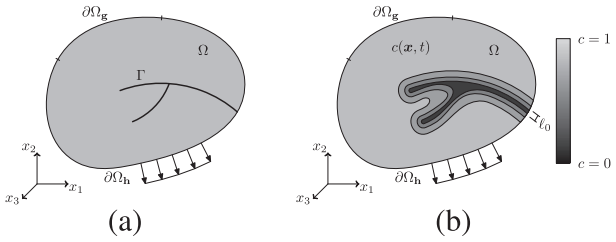


**Fig. 1.** A schematic representation of (a) a solid body $\Omega$ with an internal discontinuity boundary $\Gamma_t$ and (b) an approximation of an internal discontinuity by a phase-field $c(\mathbf{x},t)$. The model parameter $\ell_0$ controls the width of the phase-field approximation.

phase-field, $c \in [0,1]$, to represent the crack. This phase-field has a value of one away from the crack and a value of zero at the crack (see Fig. 1). The phase-field approximation introduces a crack density functional, $\Gamma_{c,n}$, that is dependent only on a length-scale parameter $\ell_0$, the phase-field $c$, and derivatives of $c$ up to order $n/2$, where $n$ is the order of the phase-field theory, such that

$$\widetilde{\Psi}_c = \int_\Omega \mathcal{G}_c \Gamma_{c,n}\, d\Omega \approx \int_\Gamma \mathcal{G}_c\, d\Gamma. \tag{4}$$

The parameter $\ell_0 \in \mathbb{R}^+$ determines the width of the approximation of the crack. It can also be considered as a material property governing the critical value of stress required for nucleation and propagation of cracks (see [6]).

*2.1.1. Second-order phase-field theory*

A crack density functional has been proposed by Bourdin et al. [10] and utilized by Miehe et al. [30] among others. This functional has the form

$$\Gamma_{c,2} = \frac{1}{4\ell_0}\left[(c-1)^2 + 4\ell_0^2|\nabla c|^2\right]. \tag{5}$$

Minimizing $\int \Gamma_{c,2}\, dx$ under the assumption that $c(0) = 0$ and $c'(x) \to 0$ as $|x| \to \infty$ leads to the Euler equation

$$c - 1 - 4\ell_0^2 \Delta c = 0. \tag{6}$$

The solution to this equation, $c$, is the solution to the minimization problem:

$$\underset{c}{\operatorname{argmin}}(I(c)), \quad I(c) = \int \Gamma_{c,2}\, dx. \tag{7}$$

In one dimension, the solution to (6) is

$$c(x) = 1 - e^{-|x|/2\ell_0}, \tag{8}$$

which is shown in Fig. 2. For this case it is easy to show that

$$\int_{-\infty}^{\infty} \mathcal{G}_c \Gamma_{c,2}\, dx = \int_\Gamma \mathcal{G}_c\, d\Gamma = \mathcal{G}_c. \tag{9}$$

In the general case (5) is used to approximate the fracture surface energy as

$$\int_\Gamma \mathcal{G}_c\, d\Gamma \approx \int_\Omega \mathcal{G}_c \left[\frac{(1-c)^2}{4\ell_0} + \ell_0|\nabla c|^2\right] d\Omega. \tag{10}$$

As (5) leads to a strong-form problem with second-order derivative of $c$, we refer to this theory as the *second-order phase-field theory*.

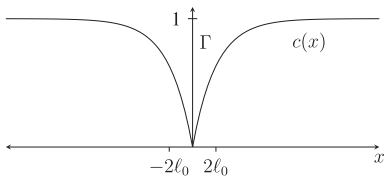


**Fig. 2.** The one-dimensional phase-field approximation to the crack surface $\Gamma = \{0\}$.

*2.1.2. Fourth-order phase-field theory*

The definition (5) is well-posed variationally for all $c \in H^1(\Omega)$. However, solutions will have, in general, no greater regularity, an example being (8). It is often the case that greater regularity in the exact solution provides better accuracy and convergence rates for numerical solutions. In this section we introduce a higher-order theory for the crack density functional that provides additional solution regularity.

We start by introducing the crack density functional with second-order derivatives of $c$

$$\Gamma_{c,4} = \frac{1}{4\ell_0}\left[(c-1)^2 + 2\ell_0^2|\nabla c|^2 + \ell_0^4(\Delta c)^2\right]. \tag{11}$$

Following the same ideas presented above we minimize $\int \Gamma_{c,4}\, d\Omega_0$, under the assumptions that $c(0) = c'(0) = 0$ and the derivatives of $c$ go to zero as $|x|$ goes to $\infty$, to get the Euler equation

$$c - 1 - 2\ell_0^2\Delta c + \ell_0^4\Delta(\Delta c) = 0. \tag{12}$$

Solving this differential equation in one dimension with $c(0) = 0,\ c'(0) = 0$, and $c'(x) \to 0$ and $c''(x) \to 0$ as $x \to \pm\infty$, we get

$$c(x) = 1 - e^{-|x|/\ell_0}\left(1 + \frac{|x|}{\ell_0}\right) \tag{13}$$

(see Fig. 3). The coefficients of (11) have been chosen such that

$$\int_{-\infty}^{\infty} \mathcal{G}_c \Gamma_{c,4}\, dx = \int_{\Gamma} \mathcal{G}_c\, d\Gamma = \mathcal{G}_c. \tag{14}$$

In the case for $d = 2$ or $d = 3$, (11) is used to approximate the fracture surface energy as

$$\int_{\Gamma} \mathcal{G}_c\, d\Gamma \approx \int_{\Omega} \mathcal{G}_c\left[\frac{(1-c)^2}{4\ell_0} + \frac{\ell_0}{2}|\nabla c|^2 + \frac{\ell_0^3}{4}(\Delta c)^2\right] d\Omega. \tag{15}$$

For this theory, (11) leads to a strong-form problem with fourth-order derivatives of $c$. Thus, we call this the *fourth-order phase-field theory*.

*2.1.3. Energy approximation*

To complete the approximation of (3) we assume the elastic strain energy density function takes the general form

$$\tilde{\psi}_e(\boldsymbol{\varepsilon}, c) = c^2\psi_e^+(\boldsymbol{\varepsilon}) + \psi_e^-(\boldsymbol{\varepsilon}). \tag{16}$$

In this form, we follow Miehe et al. [30] and let $\psi_e^+$ and $\psi_e^-$ represent an additive decomposition of $\psi_e$ that provides a distinction between energy contributions from tensile and compressive deformations, respectively (see Appendix A for details). With this, the phase-field approximation of the potential energy (3) becomes

$$\widetilde{\Psi}(\boldsymbol{\varepsilon}, c) = \int_{\Omega} c^2\psi_e^+(\boldsymbol{\varepsilon}) + \psi_e^-(\boldsymbol{\varepsilon}) d\Omega + \int_{\Omega} \mathcal{G}_c\Gamma_{c,n} d\Omega \tag{17}$$

and thus the Helmholtz free energy is given by

$$\psi_n = c^2\psi_e^+ + \psi_e^- + \mathcal{G}_c\Gamma_{c,n}. \tag{18}$$

By applying the phase-field only to the tensile part of the elastic strain energy density, we prohibit crack propagation under compression. In some cases, this feature has been observed to be important. This is particularly true for dynamic simulations, as compressive stress waves reflecting from domain boundaries tend to create physically unrealistic fracture patterns in the case where the phase-field is also applied to the compressive energy.

*2.2. Variational derivation of the phase-field fracture model*

We now derive the governing problem statements for the second- and fourth-order theories from a global energy rate balance principle. We begin by defining the rate of external work functional

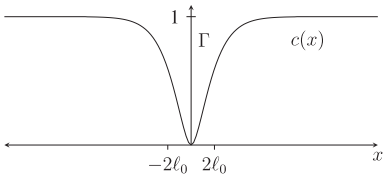


**Fig. 3.** The smooth approximation to the crack surface $\Gamma$ for the fourth-order theory.

$$\mathcal{P}_{\text{ext}}(\dot{\mathbf{u}}) = \int_{\Omega} \mathbf{b} \cdot \dot{\mathbf{u}}\, d\Omega + \int_{\partial\Omega_{\mathbf{h}}} \mathbf{h} \cdot \dot{\mathbf{u}}\, d\partial\Omega, \tag{19}$$

where $\dot{\mathbf{u}}$ is the velocity, $\mathbf{b}$ is a body force, which does not depend on displacements, and $\mathbf{h}$ is a traction vector applied to $\partial\Omega_{\mathbf{h}}$. The kinetic energy functional is given by

$$\mathcal{K}(\dot{\mathbf{u}}) = \int_{\Omega} \frac{1}{2}\rho|\dot{\mathbf{u}}|^2 d\Omega, \tag{20}$$

where $\rho$ is mass density. The rate of internal work functional is defined as

$$\mathcal{P}_{\text{int},n} = \frac{d}{dt}\int_{\Omega} \psi_n\, d\Omega, \tag{21}$$

where $\psi_n$ is defined in (18) and we will make explicit the dependent variables below. Given these definitions, and assuming no dissipation, the principle of balance of energy can be stated as

$$\frac{d}{dt}\mathcal{K} + \mathcal{P}_{\text{int},n} - \mathcal{P}_{\text{ext}} = 0. \tag{22}$$

*2.2.1. Second-order phase-field theory*

Substituting (18) into (21) and making use of (5), we can compute the rate of internal work functional for the second-order theory, which, after applying the divergence theorem and dropping explicit dependence on the primary variables $\mathbf{u}$ and $c$ for simplicity, is

$$\begin{aligned}\mathcal{P}_{\text{int},2}(\dot{\mathbf{u}},\dot{c}) &= \frac{d}{dt}\int_{\Omega}\left\{c^2\psi_e^+ + \psi_e^- + \mathcal{G}_c\left[\frac{(1-c)^2}{4\ell_0} + \ell_0|\nabla c|^2\right]\right\}d\Omega \\ &= \int_{\Omega}\left\{-\nabla\cdot\left(c^2\boldsymbol{\sigma}^+ + \boldsymbol{\sigma}^-\right)\cdot\dot{\mathbf{u}} + \left[2c\psi_e^+ + \frac{\mathcal{G}_c(c-1)}{2\ell_0} - 2\mathcal{G}_c\ell_0\Delta c\right]\dot{c}\right\}d\Omega + \int_{\partial\Omega}\left(c^2\boldsymbol{\sigma}^+ + \boldsymbol{\sigma}^-\right)\mathbf{n}\cdot\dot{\mathbf{u}}\,\partial\Omega \\ &\quad + \int_{\partial\Omega} 2\mathcal{G}_c\ell_0(\nabla c\cdot\mathbf{n})\dot{c}\, d\partial\Omega,\end{aligned} \tag{23}$$

where $\dot{c} = dc/dt$, $\mathbf{n}$ is the outward unit normal vector of the boundary, $\boldsymbol{\sigma}^+ = \partial\psi_e^+/\partial\boldsymbol{\varepsilon}$, and $\boldsymbol{\sigma}^- = \partial\psi_e^-/\partial\boldsymbol{\varepsilon}$. Letting $\ddot{\mathbf{u}} = d^2\mathbf{u}/dt^2$ be the acceleration, this leads to

$$\begin{aligned}0 &= \frac{d}{dt}\mathcal{K}(\dot{\mathbf{u}}) + \mathcal{P}_{\text{int},2}(\dot{\mathbf{u}},\dot{c}) - \mathbf{P}_{\text{ext}}(\dot{\mathbf{u}}) \\ &= \int_{\Omega}\left\{-\nabla\cdot\left(c^2\boldsymbol{\sigma}^+ + \boldsymbol{\sigma}^-\right) - \mathbf{b} + \rho\ddot{\mathbf{u}}\right\}\cdot\dot{\mathbf{u}}\, d\Omega + \int_{\Omega}\left\{2c\psi_e^+ + \frac{\mathcal{G}_c(c-1)}{2\ell_0} - 2\mathcal{G}_c\ell_0\Delta c\right\}\dot{c}\, d\Omega \\ &\quad + \int_{\partial\Omega_{\mathbf{h}}}\left\{\left(c^2\boldsymbol{\sigma}^+ + \boldsymbol{\sigma}^-\right)\mathbf{n} - \mathbf{h}\right\}\cdot\dot{\mathbf{u}}\, d\partial\Omega + \int_{\partial\Omega} 2\mathcal{G}_c\ell_0(\nabla c\cdot\mathbf{n})\dot{c}\, d\partial\Omega.\end{aligned} \tag{24}$$

We assume that this must hold for arbitrary values of $\dot{\mathbf{u}}$ and $\dot{c}$. From this, we get the strong form for the second-order initial boundary value problem, which is

$$(\text{S})\begin{cases}\nabla\cdot\boldsymbol{\sigma} + \mathbf{b} = \rho\ddot{\mathbf{u}} & \text{on} \quad \Omega\times]0,T[, \\ \frac{4\ell_0 c\psi_e^+}{\mathcal{G}_c} + c - 4\ell_0^2\Delta c = 1 & \text{on} \quad \Omega\times]0,T[, \\ \mathbf{u} = \mathbf{g} & \text{on} \quad \partial\Omega_{\mathbf{g}}\times]0,T[, \\ \boldsymbol{\sigma}\mathbf{n} = \mathbf{h} & \text{on} \quad \partial\Omega_{\mathbf{h}}\times]0,T[, \\ \nabla c\cdot\mathbf{n} = 0 & \text{on} \quad \partial\Omega\times]0,T[, \\ \mathbf{u} = \mathbf{u}_0 & \text{on} \quad \Omega\times 0, \\ \dot{\mathbf{u}} = \mathbf{v}_0 & \text{on} \quad \Omega\times 0, \\ c = c_0 & \text{on} \quad \Omega\times 0,\end{cases} \tag{25}$$

where

$$\boldsymbol{\sigma} = c^2\frac{\partial\psi_{\text{e}}^+}{\partial\boldsymbol{\varepsilon}} + \frac{\partial\psi_{\text{e}}^-}{\partial\boldsymbol{\varepsilon}}. \tag{26}$$

$\mathbf{g}$ and $\mathbf{h}$ are prescribed on $\partial\Omega_{\mathbf{g}}$ and $\partial\Omega_{\mathbf{h}}$, respectively, for all $t\in]0,T[$, and $\mathbf{n}$ is the outward unit normal vector of the boundary. The initial conditions are given by $\mathbf{u}_0$ for displacements, $\mathbf{v}_0$ for velocities, and $c_0$ for the phase-field.

**Remark 2.1.** For simplicity, we have not addressed the issue of irreversibility. There is nothing in the above formulation to prevent cracks from healing if loads are removed (the formulation is, nonetheless, thermodynamically consistent). For a discussion on how irreversibility can be enforced see Miehe et al. [30] and Borden et al. [6]. The essential idea is to replace the strain energy in the phase-field equation, for example in $(25)_2$, by a strain-energy history, $\mathcal{H}$, which acts as a threshold and which satisfies the Karush–Kuhn–Tucker loading/unloading conditions:

$$\psi_e^+ - \mathcal{H} \leqslant 0, \quad \dot{\mathcal{H}} \geqslant 0, \quad \dot{\mathcal{H}}\left(\psi_e^+ - \mathcal{H}\right) = 0. \tag{27}$$

In the monotonically forced calculations presented subsequently in this paper, whether or not we account for the strain-energy history condition, (27), has no effect on the results. It should also be noted that ignoring the strain-energy history loading/unloading does not represent any thermodynamic inconsistencies. However, accounting for the strain-energy history loading/unloading conditions does precluded crack "healing" which is physically typically warranted, although not precluded by thermodynamics.

The numerical solution of (25) requires spatial and temporal discretizations. Time is discretized by the $\alpha$ methods described in Borden et al. [6]. We formulate the spatial discretization for the second order theory by means of the semi-discrete Galerkin method.

For the weak form of the problem in $d$ dimensions we define the trial solution spaces $\boldsymbol{\mathcal{S}}_t$ for the displacements and $\widetilde{\mathcal{S}}_t$ for the phase-field as

$$\boldsymbol{\mathcal{S}}_t = \left\{\mathbf{u}(t) \in \left(H^1(\Omega)\right)^d | \mathbf{u}(t) = \mathbf{g} \text{ on } \partial\Omega_{\mathbf{g}}\right\}, \tag{28}$$

$$\widetilde{\mathcal{S}}_t = \left\{c(t) \in H^1(\Omega)\right\}. \tag{29}$$

Similarly, the weighting function spaces are defined as

$$\boldsymbol{\mathcal{V}} = \left\{\mathbf{w} \in \left(H^1(\Omega)\right)^d | \mathbf{w} = 0 \text{ on } \partial\Omega_{\mathbf{g}}\right\}, \tag{30}$$

$$\widetilde{\mathcal{V}} = \left\{q \in H^1(\Omega)\right\}. \tag{31}$$

Multiplying the equations in (25) by the weighting functions and applying integration by parts leads to the weak form:

$$\text{(W)} \begin{cases} \text{Given } \mathbf{g}, \mathbf{h}, \mathbf{b}, \mathbf{u}_0, \dot{\mathbf{u}}_0, \text{ and } c_0, \text{ find } \mathbf{u}(t) \in \boldsymbol{\mathcal{S}}_t \text{ and } c(t) \in \widetilde{\mathcal{S}}_t, t \in [0,T], \text{ such that for all} \\ \mathbf{w} \in \boldsymbol{\mathcal{V}} \text{ and for all } q \in \widetilde{\mathcal{V}}, \\ (\rho\ddot{\mathbf{u}}, \mathbf{w})_\Omega + (\boldsymbol{\sigma}, \nabla\mathbf{w})_\Omega = (\mathbf{h}, \mathbf{w})_{\partial\Omega_{\mathbf{h}}} + (\mathbf{b}, \mathbf{w})_\Omega, \\ \left(\frac{4\ell_0 c\psi_e^+}{\mathcal{G}_c} + c, q\right)_\Omega + \left(4\ell_0^2\nabla c, \nabla q\right)_\Omega = (1, q)_\Omega \\ (\rho\mathbf{u}(0), \mathbf{w})_\Omega = (\rho\mathbf{u}_0, \mathbf{w})_\Omega, \\ (\rho\dot{\mathbf{u}}(0), \mathbf{w})_\Omega = (\rho\dot{\mathbf{u}}_0, \mathbf{w})_\Omega, \end{cases} \tag{32}$$

where $(\cdot,\cdot)_\Omega$ is the $L^2$ inner product on $\Omega$.

Following the Galerkin method, we let $\boldsymbol{\mathcal{S}}_t^h \subset \boldsymbol{\mathcal{S}}_t$, $\boldsymbol{\mathcal{V}}^h \subset \boldsymbol{\mathcal{V}}$, $\widetilde{\mathcal{S}}_t^h \subset \widetilde{\mathcal{S}}_t$, and $\widetilde{\mathcal{V}}^h \subset \widetilde{\mathcal{V}}$ be the usual finite-dimensional approximations to the function spaces of the weak form (see [23] for details). The semidiscrete Galerkin form of the problem is then given as

$$\text{(G)} \begin{cases} \text{Given } \mathbf{g}, \mathbf{h}, \mathbf{b}, \mathbf{u}_0, \dot{\mathbf{u}}_0, \text{ and } c_0, \text{ find } \mathbf{u}^h(t) \in \boldsymbol{\mathcal{S}}_t^h \text{ and } c^h(t) \in \widetilde{\mathcal{S}}_t^h, t \in [0,T], \text{ such that for all } \mathbf{w}^h \in \boldsymbol{\mathcal{V}}^h \text{ and for all } q^h \in \widetilde{\mathcal{V}}^h, \\ \left(\rho\ddot{\mathbf{u}}^h, \mathbf{w}^h\right)_\Omega + \left(\boldsymbol{\sigma}, \nabla\mathbf{w}^h\right)_\Omega = \left(\mathbf{h}, \mathbf{w}^h\right)_{\partial\Omega_{\mathbf{h}}} + \left(\mathbf{b}, \mathbf{w}^h\right)_\Omega, \\ \left(\frac{4\ell_0 c^h\psi_e^+}{\mathcal{G}_c} + c^h, q^h\right)_\Omega + \left(4\ell_0^2\nabla c^h, \nabla q^h\right)_\Omega = \left(1, q^h\right)_\Omega, \\ \left(\rho\mathbf{u}^h(0), \mathbf{w}^h\right)_\Omega = \left(\rho\mathbf{u}_0, \mathbf{w}^h\right)_\Omega, \\ \left(\rho\dot{\mathbf{u}}^h(0), \mathbf{w}^h\right)_\Omega = \left(\rho\dot{\mathbf{u}}_0, \mathbf{w}^h\right)_\Omega. \end{cases} \tag{33}$$

The explicit representations of $\mathbf{u}^h$, $\mathbf{w}^h$, $c^h$, and $q^h$ in terms of the basis functions and control variables are assumed to take the form

$$\mathbf{u}^h(\mathbf{x}, t) = \sum_A^{n_b} N_A(\mathbf{x})\mathbf{u}_A(t), \tag{34}$$

$$\mathbf{w}^h(\mathbf{x}, t) = \sum_A^{n_b} N_A(\mathbf{x})\mathbf{w}_A(t), \tag{35}$$

$$c^h(\mathbf{x}, t) = \sum_A^{n_b} N_A(\mathbf{x})c_A(t), \tag{36}$$

$$q^h(\mathbf{x}, t) = \sum_A^{n_b} N_A(\mathbf{x})q_A(t), \tag{37}$$

where $n_b$ is the number of control variables, the $N_A$'s are the global basis functions, and $\mathbf{u}_A$, $\mathbf{w}_A$, $c_A$, and $q_A$ are control variable degrees-of-freedom. Note that we have assumed that both the trial solution and weighting function spaces are defined by the same set of basis functions.

*2.2.2. Fourth-order phase-field theory*

As with the second-order theory we substitute (18) into (21) but now make use of (11), so that we can compute the rate of internal work functional for the fourth-order theory, which is

$$\begin{aligned}\mathcal{P}_{\text{int},4}(\dot{\mathbf{u}},\dot{c},\nabla\dot{c}) &= \frac{d}{dt}\int_\Omega \left\{ c^2\psi_e^+ + \psi_e^- + \mathcal{G}_c\left[\frac{(1-c)^2}{4\ell_0} + \frac{\ell_0}{2}|\nabla c|^2 + \frac{\ell_0^3}{4}(\Delta c)^2\right]\right\} d\Omega \\ &= \int_\Omega -\nabla\cdot\left(c^2\boldsymbol{\sigma}^+ + \boldsymbol{\sigma}^-\right)\cdot\dot{\mathbf{u}}\, d\Omega + \int_\Omega \left\{ 2c\psi_e^+ + \frac{\mathcal{G}_c(c-1)}{2\ell_0} - \mathcal{G}_c\ell_0\Delta c + \frac{\mathcal{G}_c\ell_0^3}{2}\Delta^2 c\right\}\dot{c}\, d\Omega \\ &\quad + \int_{\partial\Omega}\left(c^2\boldsymbol{\sigma}^+ + \boldsymbol{\sigma}^-\right)\mathbf{n}\cdot\dot{\mathbf{u}}\, d\partial\Omega + \int_{\partial\Omega}\frac{\mathcal{G}_c\ell_0}{2}\left\{2\nabla c - \ell_0^2\nabla(\Delta c)\right\}\cdot\mathbf{n}\dot{c}\, d\partial\Omega + \int_{\partial\Omega}\frac{\mathcal{G}_c\ell_0^3}{2}\Delta c\nabla\dot{c}\cdot\mathbf{n}\, d\partial\Omega. \end{aligned} \tag{38}$$

We assume this must hold for arbitrary values of $\dot{\mathbf{u}}$, $\dot{c}$, and $\nabla\dot{c}\cdot\mathbf{n}$. Following the same procedure as for the second-order theory, this leads to the strong form statement of the fourth-order theory initial boundary value problem, given by

$$(\mathrm{S})\begin{cases} \nabla\cdot\boldsymbol{\sigma} + \mathbf{b} = \rho\ddot{\mathbf{u}} & \text{on } \Omega\times]0,T[, \\ \frac{4\ell_0 c\psi_e^+}{\mathcal{G}_c} + c - 2\ell_0^2\Delta c + \ell_0^4\Delta(\Delta c) = 1 & \text{on } \Omega\times]0,T[, \\ \mathbf{u} = \mathbf{g} & \text{on } \partial\Omega_{\mathbf{g}}\times]0,T[, \\ \boldsymbol{\sigma}\mathbf{n} = \mathbf{h} & \text{on } \partial\Omega_{\mathbf{h}}\times]0,T[, \\ \Delta c = 0 & \text{on } \partial\Omega\times]0,T[, \\ \nabla\left(\ell_0^4\Delta c - 2\ell_0^2 c\right)\cdot\mathbf{n} = 0 & \text{on } \partial\Omega\times]0,T[, \\ \mathbf{u} = \mathbf{u}_0 & \text{on } \Omega\times 0, \\ \dot{\mathbf{u}} = \mathbf{v}_0 & \text{on } \Omega\times 0, \\ c = c_0 & \text{on } \Omega\times 0. \end{cases} \tag{39}$$

For the weak form of the problem we define the trial solution spaces $\mathcal{S}_t$ for the displacements and $\widetilde{\mathcal{S}}_t$ for the phase-field as

$$\mathcal{S}_t = \left\{\mathbf{u}(t)\in\left(H^1(\Omega)\right)^d \,|\, \mathbf{u}(t) = \mathbf{g} \text{ on } \partial\Omega_{\mathbf{g}}\right\}, \tag{40}$$

$$\widetilde{\mathcal{S}}_t = \left\{c(t)\in H^2(\Omega)\right\}. \tag{41}$$

Similarly, the weighting function spaces are defined as

$$\mathcal{V} = \left\{\mathbf{w}\in\left(H^1(\Omega)\right)^d \,|\, \mathbf{w} = 0 \text{ on } \partial\Omega_{\mathbf{g}}\right\}, \tag{42}$$

$$\widetilde{\mathcal{V}} = \left\{q\in H^2(\Omega)\right\}. \tag{43}$$

Multiplying the equations in (39) by the appropriate variational functions and applying integration by parts leads to the weak form:

$$(\mathrm{W})\begin{cases} \text{Given } \mathbf{g},\mathbf{h},\mathbf{u}_0,\dot{\mathbf{u}}_0, \text{ and } c_0 \text{ find } \mathbf{u}(t)\in\mathcal{S}_t \text{ and } c(t)\in\widetilde{\mathcal{S}}_t, t\in[0,T], \text{ such that for all } \mathbf{w}\in\mathcal{V} \text{ and for all } q\in\widetilde{\mathcal{V}} \\ (\rho\ddot{\mathbf{u}},\mathbf{w})_\Omega + (\boldsymbol{\sigma},\nabla\mathbf{w})_\Omega = (\mathbf{h},\mathbf{w})_{\partial\Omega_{\boldsymbol{h}}}, \\ \left(\frac{4\ell_0 c\psi_e^+}{\mathcal{G}_c} + c, q\right)_\Omega + \left(2\ell_0^2\nabla c,\nabla q\right)_\Omega + \left(\ell_0^4\Delta c,\Delta q\right)_\Omega = (1,q)_\Omega, \\ (\rho\mathbf{u}(0),\mathbf{w})_\Omega = (\rho\mathbf{u}_0,\mathbf{w})_\Omega, \\ (\rho\dot{\mathbf{u}}(0),\mathbf{w})_\Omega = (\rho\dot{\mathbf{u}}_0,\mathbf{w})_\Omega. \end{cases} \tag{44}$$

The Galerkin form follows in the same way as for the second-order theory.

**Remark 2.2.** The function spaces for the displacements are not required to be as smooth as the spaces for the fourth-order phase-field. In practice, however, we typically use the same approximation spaces for both the displacement and phase-field.

*2.2.3. A note on Γ-convergence*

The notion of Γ-convergence has played an important role in establishing the second-order phase-field theory as a valid model for brittle fracture. The important Γ-convergence results related to phase-field approximations for fracture are summarized from Giovanni [21] as follows:

**Definition 2.1** ($\Gamma$-*convergence*). Let $X$ be a metric space. A sequence of functionals, $F_{\ell_0} : X \to [0,\infty],\ \ell_0 > 0$, on $X$ is said to $\Gamma$-converge to the $\Gamma$-limit $F : X \to [0,\infty]$ if and only if

- (Lower bound inequality) For every $u \in X$ and every sequence $(u_{\ell_0}) \in X$ such that $u_{\ell_0} \to u$ in $X$ as $\ell_0 \to 0$,
$$F(u) \leqslant \liminf_{\ell_0 \to 0} F_{\ell_0}(u_{\ell_0}) \tag{45}$$
- (Upper bound inequality) For every $u \in X$, there exists a sequence $(u_{\ell_0}) \in X$ converging to $u$ such that
$$F(u) \geqslant \limsup_{\ell_0 \to 0} F_{\ell_0}(u_{\ell_0}) \tag{46}$$

**Theorem 2.1.** *If $F_{\ell_0}$ $\Gamma$-converges to $F$ and $u_{\ell_0}$ minimizes $F_{\ell_0}$ over $X$, then every cluster point of $(u_{\ell_0})$ minimizes $F$ over $X$.*

In the case of the phase-field model for brittle fracture, $\Gamma$-convergence implies that the minimizing solution to $\tilde{\Psi}_c$ will converge to a minimizing solution of $\Psi$ as $\ell_0$ goes to zero. Chambolle [15] has provided a $\Gamma$-convergence proof for the case of brittle fracture in linear elasticity that shows that as $\ell_0$ approaches zero the second-order approximate potential energy

$$\tilde{\Psi}_c = \int_{\Omega_0} (c^2 + k)\psi_e(\boldsymbol{\varepsilon}) d\boldsymbol{x} + \int_{\Omega_0} \mathcal{G}_c \left[ \frac{(1-c)^2}{4\ell_0} + \ell_0 |\nabla c|^2 \right] d\boldsymbol{x}. \tag{47}$$

$\Gamma$-converges to the total potential energy for Griffith's theory given by (3). The model parameter $k \ll 1$ was introduced in Ambrosio and Tortorelli [1] as a way to avoid ill-posedness. Although it has been used in numerous numerical implementations and theoretical papers (see [4,7,9,20,8,17,25,2,13]), Braides [12] proved later it was not necessary in order to obtain $\Gamma$-convergence. We have tested the necessity of setting $k > 0$ in our formulation numerically and we have also found its inclusion to be unnecessary. In fact, all calculations presented in this paper set $k = 0$ and it has not been included in the formulations presented here.

A $\Gamma$-convergence proof for the fourth-order theory presented in Section 2.2.2 has not yet been established. However, similar theories have been introduced in the field of computer graphics and image segmentation. These theories are based on a conjecture by Giorgi [16] and also lack a complete proof. A formal description of a proof has been provided by March and Dozio [29] and a partial proof by Loreti and March [28]. A successful application of this type of approximation has been reported by Esedoglu and March [18]. In Section 3 we provide numerical evidence that the fourth-order theory presented here is well behaved at the length scales for $\ell_0$ that are practical for computing.

## 3. Analysis

In this section we analyze the phase-field model developed in Section 2. We begin with a simple one-dimensional analysis that provides insight into the convergence behavior of the strain and surface energies. It will be followed by a numerical analysis of a two-dimensional problem that will help to verify our findings for the one-dimensional study. These analyses will help to establish important properties of the fourth-order approximation presented in Section 2.1.2. We will conclude this section with a three-dimensional numerical example that demonstrates the ability of the phase-field models presented here to capture complex three-dimensional crack behavior.

### 3.1. One-dimensional cracked bar

An exact analysis of the general coupled non-linear problems presented in (25) and (39) is beyond the scope of this paper. To provide insight into the behavior of these models, however, we present here a heuristic analysis in one dimension. In this analysis, we will compare the phase-field model to the model problem shown in Fig. 4. This model problem is a bar that is fixed at its left end, cracked completely through at its center, and displaced by a distance of $u_0$ at its right end. This bar will have no strain energy and we have chosen the material parameters so that the surface energy of the fracture is equal to one. In the analysis below, we will study the convergence behavior of the strain and surface energy for the phase-field theories in relation to this model problem. For this analysis, we will uncouple the equations so that each unknown can be studied independently. Quasi-static behavior is assumed throughout.

#### 3.1.1. Strain energy approximation

We will first study the convergence behavior of the strain energy when the crack is approximated by a phase-field. For this study, we will choose a phase-field and then seek the solution to the following boundary value problem:

$$\begin{cases} \frac{d}{dx}\left(c^2 E \frac{du}{dx}\right) = 0 \quad -L < x < L, \\ u(-L) = 0, \\ u(L) = u_0. \end{cases} \tag{48}$$

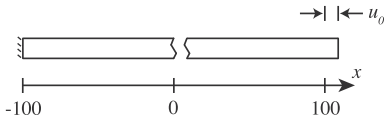


**Fig. 4.** The one-dimensional model problem for the analysis in this section is a bar fixed at the left end with a through crack at the center and displaced by a distance of $u_0$ at the right end.

For the second-order theory we choose the phase-field given by (8), shown in Fig. 2, and for the fourth-order theory we choose the phase-field given by (13), shown in Fig. 3.

The exact solution for this problem is independent of our choice of phase-field as long as $c(0) = 0$. The solution can be found by noting that $c^2 du/dx$ is constant and $c(0) = 0$. Therefore, the solution must be equal to zero. For $x \neq 0$ we know that $c(x) \neq 0$. This implies that $du/dx = 0$ for $x \neq 0$. It follows that the exact displacements are given by

$$u = \begin{cases} 0 & L \leqslant x < 0, \\ u_0 & 0 < x \leqslant L. \end{cases} \tag{49}$$

A subtle point to be aware of for this problem is that although the derivative of the displacement, $du/dx$, is not well defined at $x = 0$ the product $c^2 du/dx$ is well defined since $c(0) = 0$.

With the exact solution to (48) established, the analysis of the approximate solution will proceed as follows. For both the second- and fourth-order theories, we will introduce an interpolant of the exact displacement solution assuming small mesh size, $h$. We will then bound the interpolation error in the energy norm, and then use the best approximation property in the energy norm to provide as estimate on the rate of convergence. Numerical results will verify that the bounds are in fact sharp.

We define the strain energy norm as

$$\|u\|_e^2 = \int_{-L}^{L} c^2 \frac{1}{2} E \left(\frac{du}{dx}\right)^2 dx. \tag{50}$$

We now let $u$ be the exact solution given in (49), $\mathcal{S}^h$ be a finite-dimensional trial function space, and $u^h \in \mathcal{S}^h$ be the solution of the Galerkin finite element problem. By the best approximation property of the Galerkin method we know

$$\|u^h - u\|_e^2 \leqslant \|w^h - u\|_e^2 \quad \forall w^h \in \mathcal{S}^h. \tag{51}$$

For the second-order theory we choose $\mathcal{S}^h$ to be the set of piecewise linear functions and then prescribe the displacement interpolant to be (see Fig. 5)

$$w^h = \begin{cases} 0 & -L \leqslant x < -h, \\ \frac{u_0}{2h}(h + x) & -h \leqslant x < h, \\ u_0 & h \leqslant x \leqslant L. \end{cases} \tag{52}$$

By the best approximation property the error given by this displacement will bound the error of the Galerkin discrete solution from above. The error is computed as

$$\begin{aligned} \|w^h - u\|_e^2 &= \int_{-L}^{L} c^2 \frac{1}{2} E \left(\frac{dw^h}{dx} - \frac{du}{dx}\right)^2 dx = \int_{-L}^{0} c^2 \frac{1}{2} E \left(\frac{dw^h}{dx}\right)^2 dx + \int_{0}^{L} c^2 \frac{1}{2} E \left(\frac{dw^h}{dx}\right)^2 dx \\ &= \int_{-h}^{0} c^2 \frac{1}{2} E \left(\frac{u_0}{2h}\right)^2 dx + \int_{0}^{h} c^2 \frac{1}{2} E \left(\frac{u_0}{2h}\right)^2 dx = E \left(\frac{u_0}{2h}\right)^2 \int_{0}^{h} c^2 dx. \end{aligned} \tag{53}$$

Taking the Taylor expansion of the second-order phase-field (8) about $x = 0$ and assuming that $h$ is small so that we can ignore higher-order terms in $x$, we get $c \cong |x|/2\ell_0$. This leads to

$$\|w^h - u\|_e^2 \cong E \left(\frac{u_0}{2h}\right)^2 \int_{0}^{h} \left(\frac{x}{2\ell_0}\right)^2 dx = \frac{E}{48} \left(\frac{u_0}{\ell_0}\right)^2 h. \tag{54}$$

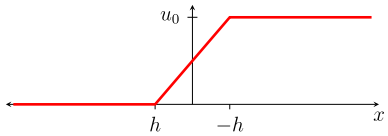


**Fig. 5.** The displacement interpolant used in the analysis of the second-order theory.

Thus, given the exact solution for the second-order phase-field theory and assuming fixed $\ell_0$, the $h$-convergence rate of the error in the strain energy norm is at least $1/2$.

A similar analysis can be carried out for the fourth-order theory. In this case we take $\mathcal{S}^h$ to be the set of piecewise quadratic functions with continuous first derivatives (e.g., quadratic B-splines) and prescribe the displacement interpolant to be (see Fig. 6).

$$w^h = \begin{cases} 0 & -L \leqslant x < -h, \\ \frac{u_0}{2h^2}(x^2 + 2hx + h^2) & -h \leqslant x < 0, \\ \frac{u_0}{2h^2}(-x^2 + 2hx + h^2) & 0 \leqslant x < h, \\ u_0 & h \leqslant x \leqslant L. \end{cases} \tag{55}$$

An upper bound estimate of the error for this interpolant is

$$\|w^h - u\|_e^2 = \int_{-h}^{0} c^2 \frac{1}{2} E\left[\frac{u_0}{h^2}(h+x)\right]^2 dx + \int_0^h c^2 \frac{1}{2} E\left[\frac{u_0}{h^2}(h-x)\right]^2 dx \leqslant E\left(\frac{u_0}{h}\right)^2 \int_0^h c^2 dx. \tag{56}$$

Following the same arguments as for the second-order case, we take the Taylor expansion of the fourth-order phase-field (13) about $x = 0$ and ignore higher-order terms in $x$ to get $c \cong x^2/2\ell_0^2$. From this we determine that

$$\|w^h - u\|_e^2 \leqslant E\left(\frac{u_0}{h}\right)^2 \int_0^h c^2 dx \cong E\left(\frac{u_0}{h}\right)^2 \int_0^h \frac{x^4}{4\ell_0^4} dx = \frac{E}{20}\left(\frac{u_0}{\ell_0^2}\right)^2 h^3. \tag{57}$$

Thus, given the exact solution for the fourth-order phase-field theory and assuming fixed $\ell_0$, the convergence rate of the error in the strain energy norm is at least $3/2$.

Fig. 7 shows convergence plots for the finite element solution to (48) with $E = 100,\ \ell_0 = 1/8,\ L = 5$ and $u_0 = 10^{-5}$. Piecewise linear basis function were used for the second-order problem and quadratic B-splines for the fourth-order problem (using quadratic B-splines for the second-order problem does not change the convergence rate). The computed results indicate that the convergence-rate estimates presented above are sharp.

The increased accuracy of the strain energy for the fourth-order model implies that the stresses will also be more accurate. Errors in the stress will lead to nonzero "cohesive tractions" inside the crack. This stress will tend to decrease the rate of crack growth.

**Remark 3.1.** These results suggest that in numerical calculations the crack will always carry some residual stress. We typically use meshes such that $\ell_0/h = 2$. At this ratio the stresses in the crack may be large enough to behave as a cohesive crack. In fact, at the length scales that can be realistically achieved for numerical calculations one might be justified in interpreting the phase-field model to be a cohesive crack model. See Verhoosel and de Borst [38] for a discussion on the use of phase-field models for cohesive fracture.

### 3.1.2. Surface energy approximation

We will now study the convergence rate of the surface energy approximation (4) for the second- and fourth-order theories. In each case we begin by computing the phase-field for a fully cracked, finite bar. We will show that when these solutions are substituted into (4), the exact surface energy is recovered as $\ell_0 \to 0$. Next, we will introduce interpolants of the exact, discontinuous displacement function of the fully cracked bar. These interpolants will be parameterized by a small positive parameter $\epsilon$ in such a way that they will converge to the exact displacement as $\epsilon \to 0$. The displacement interpolants will be used to define strain energy functions that will be substituted into the phase-field equations. The solutions will then be used to determine the convergence rates of the surface energy term as $\epsilon \to 0$. This analysis will show how the surface energy is affected by errors in the discretization of the displacements and will provide insight into the behavior of the effective critical energy release rate, defined as

$$\mathcal{G}_c^{\text{eff}} = \frac{\tilde{\Psi}_c}{a} \tag{58}$$

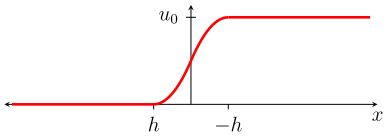


**Fig. 6.** The displacement interpolant used in the analysis of the fourth-order theory.

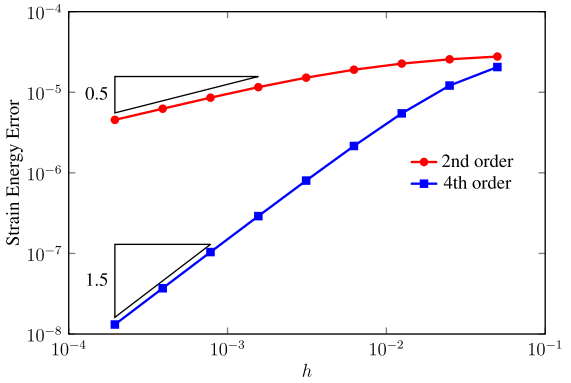


**Fig. 7.** Convergence plots for the error in the computed strain energy term.

where $\tilde{\Psi}_c$ is the energy associated with the crack surfaces in (4) and $a$ is the total crack length (in one dimension $a = 1$ for each crack). Understanding the effective critical energy release rate is important when interpreting numerical results, because it provides information about how the model over- or under-predicts crack growth.

*3.1.2.1. Second-order theory.* We begin with the second-order theory. For the fully developed crack, i.e., $du/dx = 0$ for $x \neq 0$, we assume that $c = 0$ at $x = 0$. Letting $\Omega = (-100, 100)$ we can compute the phase-field profile (for the right half of the domain) from the following boundary value problem:

$$\begin{cases} c - 4\ell_0^2 c'' = 1 & 0 < x < 100, \\ c(0) = 0, \\ c'(100) = 0. \end{cases} \tag{59}$$

Substituting the exact solution to this problem into the surface energy term, we obtain

$$\tilde{\Psi}_c = 2\mathcal{G}_c \int_0^{100} \left\{ \frac{(1-c)^2}{4\ell_0} + \ell_0 (c')^2 \right\} dx = \mathcal{G}_c \left( \frac{\exp\left(\frac{100}{\ell_0}\right) - 1}{\exp\left(\frac{100}{\ell_0}\right) + 1} \right). \tag{60}$$

It is clear from this expression that as $\ell_0$ goes to zero the right hand side goes to $\mathcal{G}_c$, i.e., we recover the exact surface energy. Even for relatively large $\ell_0$, say $\ell_0 = 1$, we get $\tilde{\Psi}_c = \mathcal{G}_c$ within machine precision and we can take $\mathcal{G}_c$ as the exact solution to facilitate computing convergence rates.

To study the approximation to (59), we define a continuous piecewise linear displacement field, shown in Fig. 8(a),

$$u = \begin{cases} 0 & x < -\epsilon, \\ \frac{u_0}{2\epsilon}(x + \epsilon) & -\epsilon \leqslant x < \epsilon, \\ u_0 & x \geqslant \epsilon, \end{cases} \tag{61}$$

where $\epsilon > 0$ is a small number and $u_0$ is the displacement at the right end of the bar shown in Fig. 4. From this, we can compute the strain, shown in Fig. 8(b), and strain energy density as

$$\frac{du}{dx} = \begin{cases} 0 & x < -\epsilon, \\ \frac{u_0}{2\epsilon} & -\epsilon < x < \epsilon, \\ 0 & x > \epsilon \end{cases} \tag{62}$$

and

$$\psi_e^+ = \begin{cases} 0 & x < -\epsilon, \\ \frac{1}{2} E \left(\frac{u_0}{2\epsilon}\right)^2 & -\epsilon < x < \epsilon, \\ 0 & x > \epsilon. \end{cases} \tag{63}$$

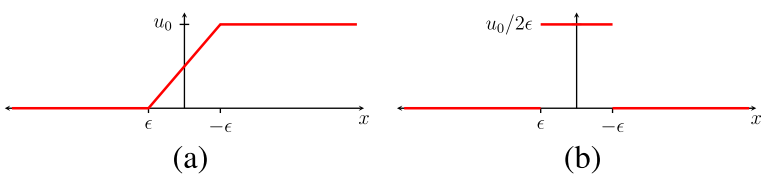


**Fig. 8.** The (a) displacement interpolant and (b) strain used in the analysis of the second-order theory.

For $x \neq 0$, $\psi_e^+ \to 0$ as $\epsilon \to 0$, and at $x = 0$ the strain becomes infinite. This is consistent with the exact solution of the cracked bar where the strain is infinite at the crack and there is no strain in the rest of the bar.

Letting $E = 10^6$ and $\mathcal{G}_c = 1$ and using (63) we seek the approximate phase-field as the solution to

$$\begin{cases} (4\ell_0\psi_e^+ + 1)c - 4\ell_0^2 c'' = 1 & -100 < x < 100, \\ c'(-100) = c'(100) = 0, \end{cases} \tag{64}$$

where we have chosen $\ell_0 = 1/8$ and $u_0 = 0.1$. This problem was solved numerically using a one-dimensional mesh of 819,200 linear finite elements. This mesh was chosen so that the convergence results depend on $\epsilon$ but are independent of mesh size, $h$. The results showing the error in the effective critical energy release rate, $\mathcal{G}_c^{\text{eff}} - \mathcal{G}_c$, are shown in Table 1. The solution converges linearly with $\epsilon$.

**Remark 3.2.** For the second-order phase-field theory, Bourdin et al. [10] showed that when discretizing with linear elements, $\tilde{\Psi}_c$ amplifies the critical energy release rate by a factor of roughly $1 + h/4\ell_0$, where $h = o(\ell_0)$. Replacing $h$ with $\epsilon$, to be consistent with the numerical results presented here, we see that these results agree well with this estimate.

*3.1.2.2. Fourth-order theory.* We follow the same strategy for the fourth-order theory. Starting with the same fully developed crack assumption as above we compute the phase-field profile from the following boundary value problem:

$$\begin{cases} c - 2\ell_0^2 c'' + \ell_0^4 c^{(4)} = 1 & 0 < x < 100, \\ c(0) = 0, \\ c'(0) = 0, \\ c''(100) = 0, \\ \ell_0^2 c^{(3)}(100) - 2c'(100) = 0. \end{cases} \tag{65}$$

Substituting the solution to this problem into the surface energy term we get

$$\tilde{\Psi}_c = 2\mathcal{G}_c \int_0^{100} \left\{ \frac{(1-c)^2}{4\ell_0} + \frac{\ell_0}{2}(c')^2 + \frac{\ell_0^3}{4}(c'')^2 \right\} dx = 2\mathcal{G}_c \left( \frac{3\ell_0^2 \exp\left(\frac{400}{\ell_0}\right) - 400\ell_0 \exp\left(\frac{200}{\ell_0}\right) - 3\ell_0^2}{6\ell_0^2 \exp\left(\frac{400}{\ell_0}\right) + 20\exp\left(\frac{200}{\ell_0}\right)(4000 + \ell_0^2) + 6\ell_0^2} \right). \tag{66}$$

Again, taking the limit of this expression as $\ell_0 \to 0$ we get $\tilde{\Psi} \to \mathcal{G}_c$, and $\tilde{\Psi} = \mathcal{G}_c$ within machine precision for the value of $\ell_0 = 1/8$ used in the calculations that follow.

The numerical solution of the fourth-order theory requires a basis with continuous first derivatives. Assuming, for convenience, a displacement field that is in the same function space as the phase-field we define a piecewise quadratic displacements field, shown in Fig. 9(a),

$$u = \begin{cases} 0 & x < -\epsilon, \\ \frac{u_0}{2\epsilon^2}(x^2 + 2\epsilon x + \epsilon^2) & -\epsilon \leqslant x < 0, \\ \frac{u_0}{2\epsilon^2}(-x^2 + 2\epsilon x + \epsilon^2) & 0 \leqslant x < \epsilon, \\ u_0 & x \geqslant \epsilon, \end{cases} \tag{67}$$

where $\epsilon$ and $u_0$ are the same parameters as used for the analysis of the second-order theory. From this we compute the strain, shown in Fig. 9(b), and strain energy density as

$$\frac{du}{dx} = \begin{cases} 0 & x < -\epsilon, \\ \frac{u_0}{\epsilon^2}(\epsilon + x) & -\epsilon \leqslant x < 0, \\ \frac{u_0}{\epsilon^2}(\epsilon - x) & 0 \leqslant x < \epsilon, \\ 0 & x \geqslant \epsilon \end{cases} \tag{68}$$

**Table 1**
Error in the computed surface energy for the one-dimensional problems given by (64) and (70). For these results we have used $\ell_0 = 1/8$.

| $\epsilon$ | 2nd-order | | 4th-order | |
|---|---|---|---|---|
| | $\mathcal{G}_c^{\text{eff}} - \mathcal{G}_c$ | Conv. rate | $\mathcal{G}_c^{\text{eff}} - \mathcal{G}_c$ | Conv. rate |
| $\ell_0$ | $4.924 \times 10^{-1}$ | | $3.448 \times 10^{-1}$ | |
| $\ell_0/2$ | $2.462 \times 10^{-1}$ | 1.000 | $1.537 \times 10^{-1}$ | 1.116 |
| $\ell_0/4$ | $1.231 \times 10^{-1}$ | 1.000 | $6.492 \times 10^{-2}$ | 1.243 |
| $\ell_0/8$ | $6.160 \times 10^{-2}$ | 0.999 | $2.479 \times 10^{-2}$ | 1.389 |
| $\ell_0/16$ | $3.085 \times 10^{-2}$ | 0.998 | $6.692 \times 10^{-3}$ | 1.889 |
| $\ell_0/32$ | $1.548 \times 10^{-2}$ | 0.995 | $8.640 \times 10^{-4}$ | 2.953 |
| $\ell_0/64$ | $7.772 \times 10^{-3}$ | 0.994 | $6.571 \times 10^{-5}$ | 3.717 |
| $\ell_0/128$ | $3.896 \times 10^{-3}$ | 0.996 | $7.248 \times 10^{-6}$ | 3.180 |

and

$$\psi_e^+ = \begin{cases} 0 & x < -\epsilon, \\ \frac{1}{2}E\left[\frac{u_0}{\epsilon^2}(\epsilon + x)\right]^2 & -\epsilon \leqslant x < 0, \\ \frac{1}{2}E\left[\frac{u_0}{\epsilon^2}(\epsilon - x)\right]^2 & 0 \leqslant x < \epsilon, \\ 0 & x \geqslant \epsilon. \end{cases} \tag{69}$$

Again, for $x \neq 0$, $\psi_e^+ \to 0$ as $\epsilon \to 0$, and at $x = 0$ the strain converges to infinity.

Letting $E = 10^6$ and $\mathcal{G}_c = 1$, the approximate phase-field satisfies the following equations, in which $\psi_e^+$ is given by (69):

$$\begin{cases} (4\ell_0\psi_e^+ + 1)c - 2\ell_0^2 c'' + \ell_0^4 c^{(4)} = 1 & -100 < x < 100, \\ c''(-100) = c''100) = 0, \\ \ell_0^2 c^{(3)}(-100) - 2c'(-100) = 0, \\ \ell_0^2 c^{(3)}(100) - 2c'(100) = 0. \end{cases} \tag{70}$$

The boundary conditions are those given in the strong form (39). This problem was discretized using one-dimensional quadratic B-splines with 819,200 uniform knot spans and solved for $\ell_0 = 1/8$ and $u_0 = 0.1$, as before. The error in the effective critical energy release rate, $\mathcal{G}_c^{\text{eff}} - \mathcal{G}_c$, is presented in Table 1 and Fig. 10. These results indicate that the $\epsilon$-convergence rate of the error in the surface energy for the fourth-order theory is approximately 3.

**Remark 3.3.** Given the piecewise constant strain in (62), it is possible to find the exact solutions to (64). The errors computed from the exact solution agree with the numerical solution up to the number of digits shown in the table above.

### 3.2. Double cantilever beam

In this section we present results for simulations of the two-dimensional double cantilever beam problem shown in Fig. 11. We use this example to study the behavior of the second- and fourth-order models at what we believe are practical length scales. That is, the dimensions and model parameters are chosen such that the scale of the geometry is about two orders of magnitude larger than $\ell_0$ and the mesh resolution is coarse enough for reasonable computation times. Another important attribute of this problem is that when displacement boundary conditions are applied, as shown in the Fig. 11, the crack growth is stable, i.e., small increases in displacements lead to small increases in crack length.

The material properties used for the analyses in this section are shown in Table 2 and plane strain and quasi-static conditions are assumed. We also assume that the solution is dominated by tensile strains and, for simplicity, use a strain energy with no additive split, i.e., $\psi_e^+ = \psi_e$ and $\psi_e^- = 0$.

In all cases, the mesh is constructed as a $C^1$-continuous quadratic hierarchical B-spline (see [39,36] for a discussion of hierarchical B-splines). There are no mesh discontinuities at the crack. Hierarchical B-splines have been used to allow local refinement of the discrete basis in the area where the crack forms. The Bézier representation (see [5,37]) of the coarsest mesh is shown in Fig. 12.

In order to initiate phase-field localization we set a Dirichlet condition on the phase-field so that $c = 0$ at $x = y = 0$. With the initial crack established, the left ends are displaced as shown in Fig. 11. For a given displacement, we define the crack tip as the largest $x$ coordinate of the phase-field contour for $c = 0.2$. The initial crack tip $a_0$ is defined by the displacement $u_0 = 0.21$. The displacement is then increased by $\Delta u = 0.02$ and the location of the crack tip is measured again. We then measure the change in crack length, $\Delta a$, and compute the change in surface energy, $\Delta\widetilde{\Psi}_c = \widetilde{\Psi}_c(u_0 + \Delta u) - \widetilde{\Psi}_c(u_0)$ with

$$\widetilde{\Psi}_c = \int_\Omega \mathcal{G}_c \Gamma_{c,n}\, d\mathbf{x}. \tag{71}$$

This procedure was followed for four levels of local mesh refinement, $h_{\min} = \{\ell_0/2, \ell_0/4, \ell_0/8, \ell_0/16\}$. The data computed for each case are shown in Table 3. Notice that both the initial crack length and change in crack length is larger for the fourth-order theory when compared to the second-order theory. This agrees with the results from the one-dimensional analysis in the previous section, which implied that the stresses are more accurate for the fourth-order model, i.e., the non-zero "cohesive tractions" in the crack are smaller. This allows the crack to grow further for a given $u$.

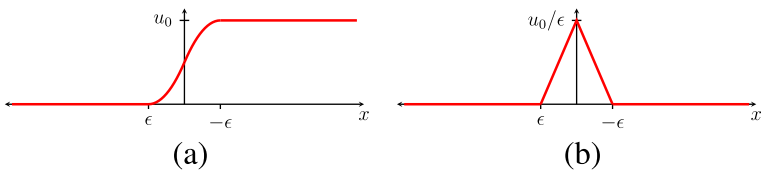


**Fig. 9.** The (a) displacement interpolant and (b) strain used in the analysis of the fourth-order theory.

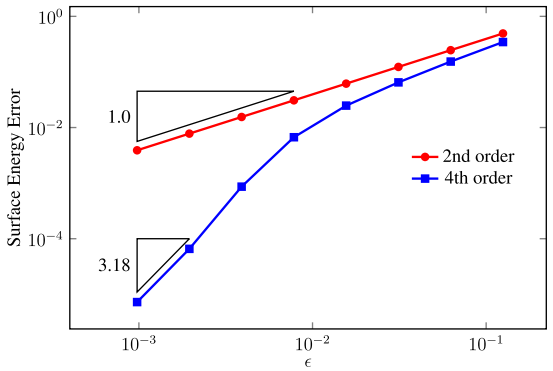


**Fig. 10.** Convergence plots for the error in the computed surface energy for the one-dimensional problems given by (64) and (70).

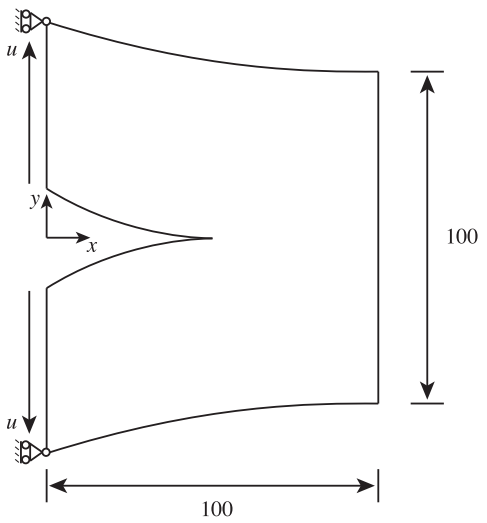


**Fig. 11.** The geometry and boundary conditions for the double cantilever beam problem. The upper and lower corners at the left edge are constrained in the $x$ direction to prevent rotation of the model and maintain symmetry.

**Table 2**
Material properties.

| Property | Value |
|---|---|
| E | 100 |
| $\nu$ | 0.25 |
| $\mathcal{G}_c$ | 0.01 |
| $\ell_0$ | 1/2 |

Table 4 shows convergence of $\mathcal{G}_c^{\text{eff}}$ measured at the displacement $u_0$. It is apparent that both models are over-predicting the critical energy release rate. There will be contributions to the surface energy term from the area away from the crack where there are non-zero strains. In particular, all of the strains that accumulated prior to the crack propagating also contribute to this term and result in a higher effective critical energy release rate.

Table 5 presents convergence data for $\mathcal{G}_c^{\text{eff}}$ corresponding to an incremental change in the displacement $\Delta u$. In this case, the contributions from strains away from the crack have less of an effect because the body is already under load. We can see that the fourth-order model is converging to a value slightly smaller than the material parameter (an extrapolation of the results for the second-order model shows the same behavior but there is too little data to make a strong claim about this). We recall that the fourth-order model was designed to give the correct surface energy for the one-dimensional problem. This example shows that this is not the case for higher dimensions. The actual surface energy that the model converges to will most likely be dependent on the length scale $\ell_0$ and other factors (geometry, number of cracks, load conditions, etc.), but it will likely converge from above and at practical mesh scales over predict the critical energy release rate.

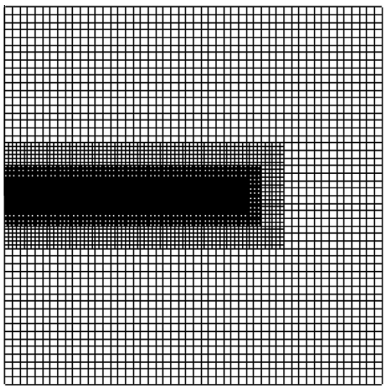

**Fig. 12.** The Bézier representation of the coarsest hierarchical B-spline mesh used to compute the results for the double cantilever beam example.

**Table 3**
Mesh refinement studies for the phase-field models of the double cantilever beam. The crack tip, $a$, is taken as the contour of the phase-field at $c = 0.2$.

| $h_{\min}$ | $a_0$ | $\Delta a$ | $\bar{\Psi}_{c,0} = \bar{\Psi}_c(u_0)$ | $\Delta\bar{\Psi}_c$ |
|---|---|---|---|---|
| *2nd-order* | | | | |
| $\ell_0/2$ | 44.340 | 4.089 | 0.526807 | 0.051357 |
| $\ell_0/4$ | 46.275 | 4.334 | 0.511438 | 0.048888 |
| $\ell_0/8$ | 47.359 | 4.480 | 0.503250 | 0.047623 |
| $\ell_0/16$ | 47.936 | 4.559 | 0.499903 | 0.046979 |
| *4th-order* | | | | |
| $\ell_0/2$ | 46.780 | 4.309 | 0.497741 | 0.047715 |
| $\ell_0/4$ | 48.073 | 4.541 | 0.492978 | 0.046325 |
| $\ell_0/8$ | 48.457 | 4.625 | 0.493001 | 0.046302 |
| $\ell_0/16$ | 48.539 | 4.645 | 0.493151 | 0.046375 |

**Table 4**
Convergence of $\mathcal{G}_c^{\text{eff}}$ for the crack tip measured at displacement $u_0$. The column labeled $\Delta\mathcal{G}_c^{\text{eff}}$ shows the difference between two consecutive measurements of $\mathcal{G}_c^{\text{eff}}$. For reference, we also show the relative error compared to the input material parameter $\mathcal{G}_c$.

| $h_{\min}$ | $\mathcal{G}_c^{\text{eff}} = \frac{\bar{\Psi}_{c,0}}{a_0}$ | $\Delta\mathcal{G}_c^{\text{eff}}$ | Conv. rate | $\frac{\mathcal{G}_c^{\text{eff}} - \mathcal{G}_c}{\mathcal{G}_c}$ |
|---|---|---|---|---|
| *2nd-order* | | | | |
| $\ell_0/2$ | 0.01188 | | | 0.188 |
| $\ell_0/4$ | 0.01105 | 0.00083 | | 0.105 |
| $\ell_0/8$ | 0.01063 | 0.00042 | 0.98 | 0.063 |
| $\ell_0/16$ | 0.01041 | 0.00022 | 0.93 | 0.041 |
| *4th-order* | | | | |
| $\ell_0/2$ | 0.01064 | | | 0.064 |
| $\ell_0/4$ | 0.01026 | 0.00038 | | 0.026 |
| $\ell_0/8$ | 0.01017 | 0.00009 | 2.08 | 0.017 |
| $\ell_0/16$ | 0.01016 | 0.00001 | 3.17 | 0.016 |

**Remark 3.4.** One of the difficulties associated with phase-field models for fracture is defining the crack tip. In these calculation we have defined the crack surfaces to be at the phase-field contour $c = 0.2$ and the tip was located through a post-processing step.

### *3.3. Three-dimensional model with random nucleation sites*

This final example demonstrates that phase-field models have the potential to become a predictive tool for complex three-dimensional crack initiation and propagation problems.

The geometry for this example is a rectangular block that is 0.01 m high by 0.01 m wide by 0.005 m deep. Several nucleation sites—spherical areas where an initial phase-field value close to zero is imposed—are randomly distributed throughout the body (see Fig. 13(a)). These sites create a representation of an inhomogeneous material and allow stress concentrations

**Table 5**
Convergence of $\mathcal{G}_c^{\text{eff}}$ for the change in crack length $\Delta a$. For reference, we also show the relative error compared to the input material parameter $\mathcal{G}_c$.

| $h_{\min}$ | $\mathcal{G}_c^{\text{eff}} = \frac{\Delta \Psi_c}{\Delta a}$ | $\Delta \mathcal{G}_c^{\text{eff}}$ | Conv. rate | $\frac{\mathcal{G}_c^{\text{eff}} - \mathcal{G}_c}{\mathcal{G}_c}$ |
|---|---|---|---|---|
| *2nd-order* | | | | |
| $\ell_0/2$ | 0.01256 | | | 0.256 |
| $\ell_0/4$ | 0.01128 | 0.00128 | | 0.128 |
| $\ell_0/8$ | 0.01063 | 0.00065 | 0.98 | 0.063 |
| $\ell_0/16$ | 0.01030 | 0.00033 | 0.98 | 0.030 |
| *4th-order* | | | | |
| $\ell_0/2$ | 0.01107 | | | 0.107 |
| $\ell_0/4$ | 0.01020 | 0.00087 | | 0.020 |
| $\ell_0/8$ | 0.01001 | 0.00019 | 2.19 | 0.001 |
| $\ell_0/16$ | 0.00998 | 0.00003 | 2.66 | −0.002 |

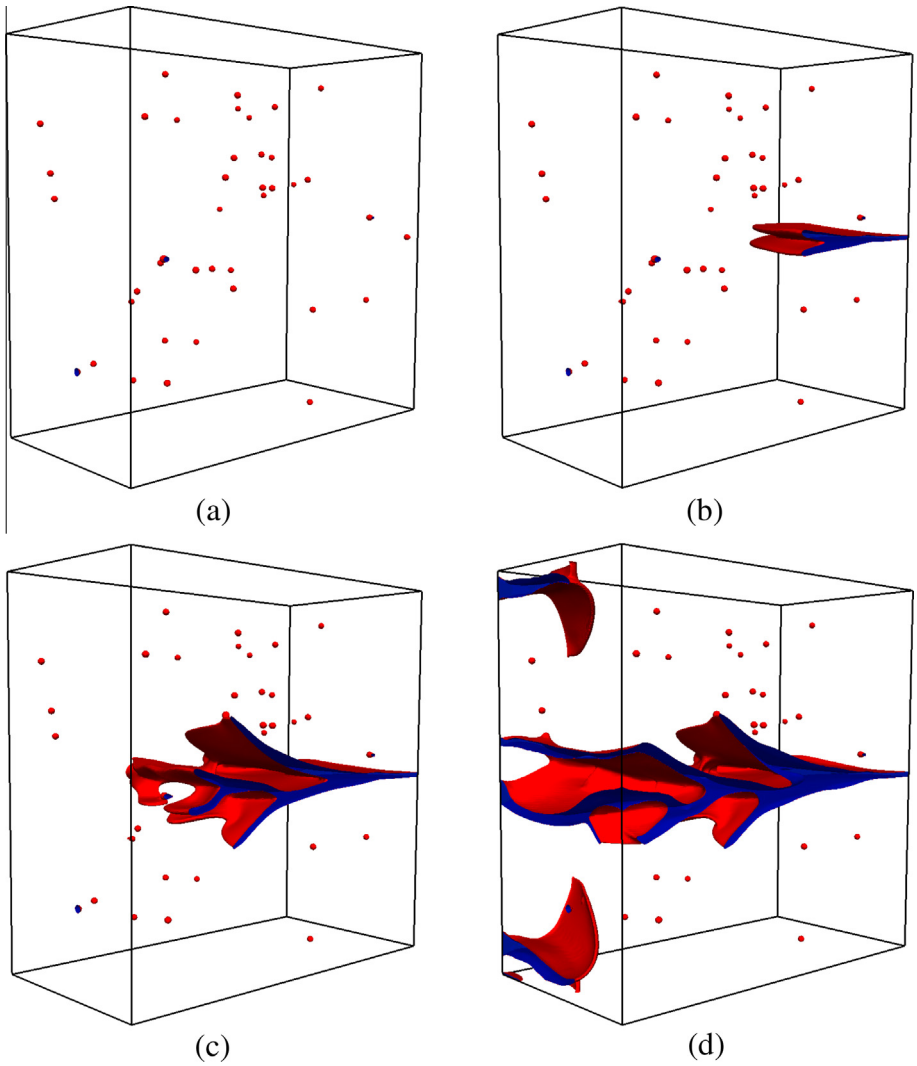


**Fig. 13.** Three-dimensional crack propagation over time. The isosurface of the phase-field for $c = 0.1$ is shown in red. The blue shading indicates the area interior to this isosurface. The initial geometry (a) is seeded with randomly distributed nucleation sites and then a displacement is applied to the top and bottom surfaces of the rectangular block. The progression of the crack from (b) to (d) shows the ability of the phase-field model to capture branching, turning, and merging of cracks in three dimensions. (For interpretation of the references to color in this figure legend, the reader is referred to the web version of this article.)

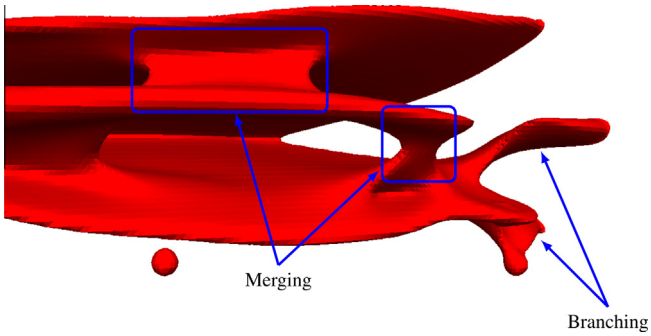


**Fig. 14.** A detailed snapshot of the crack evolution in three-dimension. Areas where the crack front is branching and merging are highlighted.

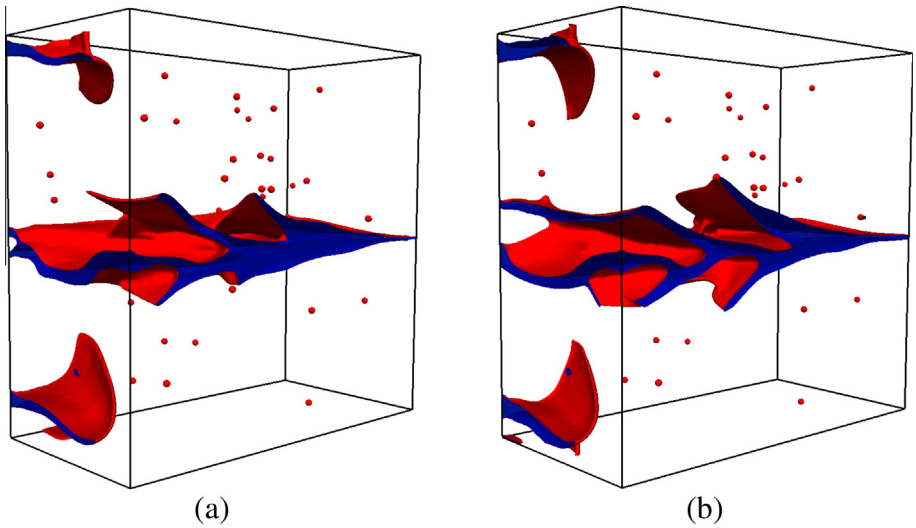


**Fig. 15.** A comparison of the second-order theory (a) and the fourth-order theory (b) for a three-dimensional problem. The fourth-order theory produces a more detailed crack pattern with longer branches.

to develop. A displacement boundary condition is imposed on the top and bottom surfaces by applying a velocity, $v$, in the direction normal to the surfaces where

$$v = \begin{cases} \frac{t}{2.5\ \mu s} 2.5\ \text{m/s} & t \leqslant 2.5\ \mu s \\ 2.5\ \text{m/s} & t > 2.5\ \mu s. \end{cases} \tag{72}$$

We use the fourth-order small strain brittle formulation introduced in Section 2.1.2 and the geometry is discretized by a singe quadratic B-spline patch with 16,384,000 uniform Bézier elements ($h = \ell_0/2$). The model parameters are $\rho = 8000$ kg/m$^3$, $E = 190$ GPa, $\nu = 0.3$, and $\mathcal{G}_c = 2.213 \times 10^4$ J/m$^2$ and the length scale was chosen to be $\ell_0 = 6.25 \times 10^{-5}$ m. Time integration of the momentum equation is performed using the explicit HHT-$\alpha$ method described by Borden et al. [6] with $\alpha = -0.3$ (see also [23] for background).

A sequence of figures showing the crack growth over time for this problem is presented in Fig. 13(a)–(d). The initial randomly distributed nucleation sites are shown in Fig. 13(a). Fig. 13(b) shows the crack beginning to propagate from one of the nucleation sites and the development of a bifurcation. In Fig. 13(c) and (d) we see multiple bifurcations developing as the crack progresses and separate branches of the crack merging. We also see additional crack fronts developing and changing direction in the upper and lower corners on the left side of the block. A detailed snapshot of the crack progression is shown in Fig. 14. Here we can see separate crack fronts merging as well as the development of complex branching patterns.

In Fig. 15 we compare the results of the fourth-order theory (Fig. 15(b)) with results produced by the second-order theory (Fig. 15(a)) for identical initial and loading conditions. The fourth-order theory produces a more detailed crack pattern with the crack branches propagating further, which is consistent with the results for the double cantilever beam.

This example illustrates that phase-field theories are able to model complex three-dimensional fracture processes. We reiterate that all of the behavior of the cracks is completely determined by the coupled momentum and phase-field

equations. There are no ad hoc rules to determine when a crack propagates, bifurcates, merges with another crack, or changes direction. These properties result in a remarkably simple, stable and robust numerical method.

## 4. Conclusions

In this paper we have introduced a fourth-order phase-field theory for fracture. This theory provides increased regularity in the exact solution of the phase-field equation, improves convergence rates for numerical solutions and opens the door to higher-order convergence rates for fracture problems. However, to exploit this attribute of the theory, one requires at least $C^1$-continuous basis functions. We utilize $C^1$-continuous hierarchically refined B-splines for this purpose. Within the isogeometric framework, the cost associated with additional smoothness requirements is minimal. We have shown that the fourth-order model improves the accuracy and convergence of the effective critical energy release rate and the strain energy. We have also concluded from these results that the stress is more accurate for the fourth-order theory. This increased accuracy leads to smaller residual stresses inside the crack and, in turn, engenders increased crack growth rates. We have also shown that both the second- and fourth-order phase-field models are capable of capturing complex crack behavior in three dimensions, including nucleation, bifurcation, and crack merging.

## Acknowledgments

This work was supported by Grants from the Office of Naval Research under contract number N00014-08-1-0992 and the Army Research Office under contract number W911NF-10-1-0216. This support is gratefully acknowledged.

The authors also acknowledge the Texas Advanced Computing Center (TACC) at The University of Texas at Austin for providing HPC and visualization resources that have contributed to the research results reported within this paper. URL: http://www.tacc.utexas.edu.

## Appendix A. Tension/compression split of the strain energy

The positive and negative components of the strain tensor are defined through a spectral decomposition of strain. Let

$$\boldsymbol{\varepsilon} = \mathbf{P}\boldsymbol{\Lambda}\mathbf{P}^T, \tag{73}$$

where $\mathbf{P}$ consists of the orthonormal eigenvectors of $\boldsymbol{\varepsilon}$ and $\boldsymbol{\Lambda} = \operatorname{diag}(\lambda_1, \lambda_2, \lambda_3)$ is a diagonal matrix of principal strains. We define

$$\boldsymbol{\varepsilon}^+ = \mathbf{P}\boldsymbol{\Lambda}^+\mathbf{P}^T, \tag{74}$$

$$\boldsymbol{\varepsilon}^- = \mathbf{P}\boldsymbol{\Lambda}^-\mathbf{P}^T, \tag{75}$$

where

$$\boldsymbol{\Lambda}^+ = \operatorname{diag}(\langle\lambda_1\rangle, \langle\lambda_2\rangle, \langle\lambda_3\rangle), \tag{76}$$

$$\boldsymbol{\Lambda}^- = \boldsymbol{\Lambda} - \boldsymbol{\Lambda}^+ \tag{77}$$

and

$$\langle x\rangle = \begin{cases} x & x > 0, \\ 0 & x \leqslant 0. \end{cases} \tag{78}$$

Then

$$\psi_e^+(\boldsymbol{\varepsilon}) = \frac{1}{2}\lambda\langle \operatorname{tr}\boldsymbol{\varepsilon}\rangle^2 + \mu \operatorname{tr}[(\boldsymbol{\varepsilon}^+)^2] \tag{79}$$

and

$$\psi_e^-(\boldsymbol{\varepsilon}) = \frac{1}{2}\lambda(\operatorname{tr}\boldsymbol{\varepsilon} - \langle \operatorname{tr}\boldsymbol{\varepsilon}\rangle)^2 + \mu \operatorname{tr}[(\boldsymbol{\varepsilon} - \boldsymbol{\varepsilon}^+)^2]. \tag{80}$$

A robust and efficient algorithm for computing the eigenvalues and eigenvectors of $3 \times 3$ symmetric matrices has been reported by Scherzinger and Dohrmann [35].

## References

[1] L. Ambrosio, V.M. Tortorelli, On the approximation of free discontinuity problems, Boll. Unione Mat. Ital. B (7) 6 (1) (1992) 105–123.
[2] H. Amor, J.J. Marigo, C. Maurini, Regularized formulation of the variational brittle fracture with unilateral contact: numerical experiments, J. Mech. Phys. Solids 57 (8) (2009) 1209–1229.
[3] I. Babuška, J.M. Melenk, The partition of unity method, Int. J. Numer. Methods Eng. 40 (4) (1997) 727–758.
[4] G. Bellettini, A. Coscia, Discrete approximation of a free discontinuity problem, Numer. Funct. Anal. Optim. 15 (3-4) (1994) 201–224.

[5] M.J. Borden, M.A. Scott, J.A. Evans, T.J.R. Hughes, Isogeometric finite element data structures based on Bézier extraction of NURBS, Int. J. Numer. Methods Eng. 87 (1-5) (2011) 15–47.
[6] M.J. Borden, C.V. Verhoosel, M.A. Scott, T.J.R. Hughes, C.M. Landis, A phase-field description of dynamic brittle fracture, Comput. Methods Appl. Mech. Eng. 217–220 (2012) 77–95.
[7] B. Bourdin, Image segmentation with a finite element method, ESAIM: Math. Model. Numer. Anal. 33 (2) (1999) 229–244.
[8] B. Bourdin, Numerical implementation of the variational formulation for quasi-static brittle fracture, Interfaces Free Bound. 9 (3) (2007) 411–430.
[9] B. Bourdin, G.A. Francfort, J-J. Marigo, Numerical experiments in revisited brittle fracture, J. Mech. Phys. Solids 48 (4) (2000) 797–826.
[10] B. Bourdin, G.A. Francfort, J-J. Marigo, The variational approach to fracture, J. Elast. 91 (1-3) (2008) 5–148.
[11] B. Bourdin, C. Larsen, C. Richardson, A time-discrete model for dynamic fracture based on crack regularization, Int. J. Fract. 168 (2) (2011) 133–143.
[12] A. Braides, Approximation of Free-Discontinuity Problems, Springer, Berlin, 1998.
[13] S. Burke, C. Ortner, E. Süli, An adaptive finite element approximation of a variational model of brittle fracture, SIAM J. Numer. Anal. 48 (3) (2010) 980–1012.
[14] G.T. Camacho, M. Ortiz, Computational modelling of impact damage in brittle materials, Int. J. Solids Struct. 33 (20-22) (1996) 2899–2938.
[15] A. Chambolle, An approximation result for special functions with bounded deformation, J. Math. Pures Appl. 83 (7) (2004) 929–954.
[16] E. de Giorgi, Some remarks on $\Gamma$-convergence and least squares method, in: G. Dal Maso, G.F. Dell'Antonio (Eds.), Composite Media and Homogenization Theory, Birkhäuser, Boston, 1991, pp. 135–142.
[17] G. Del Piero, G. Lancioni, R. March, A variational model for fracture mechanics: numerical experiments, J. Mech. Phys. Solids 55 (12) (2007) 2513–2537.
[18] S. Esedoglu, R. March, Segmentation with depth but without detecting junctions, J. Math. Imag. Vision 18 (2002) 7–15.
[19] G.A. Francfort, J-J. Marigo, Revisiting brittle fracture as an energy minimization problem, J. Mech. Phys. Solids 46 (8) (1998) 1319–1342.
[20] A. Giacomini, Ambrosio–Tortorelli approximation of quasi-static evolution of brittle fractures, Calc. Var. Partial Differ. Equ. 22 (2) (2005) 129–172.
[21] A. Giovanni, Variational models for phase transitions, an approach via $\Gamma$-convergence, in: G. Buttazzo, A. Marino, M.K.V. Murthy (Eds.), Calculus of Variations and Partial Differential Equations, Topics on Geometrical Evolution Problems and Degree Theory, Springer-Verlag, Berlin-Heidelberg, 2000, pp. 95–114.
[22] M. Hofacker, C. Miehe, A phase field model of dynamic fracture: robust field updates for the analysis of complex crack patterns, Int. J. Numer. Methods Eng. 93 (3) (2013) 276–301.
[23] T.J.R. Hughes, The Finite Element Method: Linear Static and Dynamic Finite Element Analysis, Dover Publications, Mineola, NY, 2000.
[24] T.J.R. Hughes, J.A. Cottrell, Y. Bazilevs, Isogeometric analysis: CAD, finite elements, NURBS, exact geometry and mesh refinement, Comput. Methods Appl. Mech. Eng. 194 (2005) 4135–4195.
[25] G. Lancioni, G. Royer-Carfagni, The variational approach to fracture mechanics. A practical application to the French Panthéon in Paris, J. Elast. 95 (1) (2009) 1–30.
[26] C.J. Larsen, Models for dynamic fracture based on Griffith's criterion, in: K. Hackl (Ed.), IUTAM Symposium on Variational Concepts with Applications to the Mechanics of Materials, vol. 21, Springer, Netherlands, 2010, pp. 131–140.
[27] C.J. Larsen, C. Ortner, E. Süli, Existence of solutions to a regularized model of dynamic fracture, Math. Methods Models Appl. Sci. 20 (7) (2010) 1021–1048.
[28] P. Loreti, R. March, Propagation of fronts in a nonlinear fourth order equation, Eur. J. Appl. Math. 11 (2) (2000) 203–213.
[29] R. March, M. Dozio, A variational method for the recovery of smooth boundaries, Image Vision Comput. 15 (9) (1997) 705–712.
[30] C. Miehe, M. Hofacker, F. Welschinger, A phase field model for rate-independent crack propagation: robust algorithmic implementation based on operator splits, Comput. Methods Appl. Mech. Eng. 199 (45–48) (2010) 2765–2778.
[31] C. Miehe, F. Welschinger, M. Hofacker, Thermodynamically consistent phase-field models of fracture: variational principles and multi-field FE implementations, Int. J. Numer. Methods Eng. 83 (10) (2010) 1273–1311.
[32] N. Moës, J. Dolbow, T. Belytschko, A finite element method for crack growth without remeshing, Int. J. Numer. Methods Eng. 46 (1) (1999) 131–150.
[33] D. Mumford, J. Shah, Optimal approximations by piecewise smooth functions and associated variational problems, Commun. Pure Appl. Math. 42 (5) (1989) 577–685.
[34] J.J.C. Remmers, R. de Borst, A. Needleman, A cohesive segments method for the simulation of crack growth, Comput. Mech. 31 (1) (2003) 69–77.
[35] W.M. Scherzinger, C.R. Dohrmann, A robust algorithm for finding the eigenvalues and eigenvectors of $3 \times 3$ symmetric matrices, Comput. Methods Appl. Mech. Eng. 197 (45-48) (2008) 4007–4015.
[36] D. Schillinger, L. Dedè, M.A. Scott, J.A. Evans, M.J. Borden, E. Rank, T.J.R. Hughes, An isogeometric design-through-analysis methodology based on adaptive hierarchical refinement of NURBS, immersed boundary methods, and T-spline CAD surfaces, Comput. Methods Appl. Mech. Eng. 249-252 (2012) 116–150.
[37] M.A. Scott, M.J. Borden, C.V. Verhoosel, T.W. Sederberg, T.J.R. Hughes, Isogeometric finite element data structures based on Bézier extraction of T-splines, Int. J. Numer. Methods Eng. 88 (2) (2011) 126–156.
[38] C.V. Verhoosel, R. de Borst, A phase-field model for cohesive fracture, Int. J. Numer. Methods Eng. 96 (1) (2013) 43–62.
[39] A.-V. Vuong, C. Giannelli, B. Jüttler, B. Simeon, A hierarchical approach to adaptive local refinement in isogeometric analysis, Comput. Methods Appl. Mech. Eng. 200 (49-52) (2011) 3554–3567.
[40] X.-P. Xu, A. Needleman, Numerical simulations of fast crack growth in brittle solids, J. Mech. Phys. Solids 42 (9) (1994) 1397–1434.